Cell

Identification of Stem Cell Populations in Sweat Glands and Ducts Reveals Roles in Homeostasis and Wound Repair

Catherine P. Lu,[2] Lisa Polak,[2] Ana Sofia Rocha,[3] H. Amalia Pasolli,[2] Shann-Ching Chen,[4] Neha Sharma,[3] Cedric Blanpain,[3] and Elaine Fuchs[1,2,*]
[1]Howard Hughes Medical Institute
[2]Laboratory of Mammalian Cell Biology & Development
The Rockefeller University, New York, NY 10065, USA
[3]IRIBHM, Université Libre de Bruxelles, Brussels 1050, Belgium
[4]Department of Pathology, St. Jude Children's Research Hospital, Memphis, TN 38105, USA
*Correspondence: fuchslb@rockefeller.edu
http://dx.doi.org/10.1016/j.cell.2012.04.045

SUMMARY

Sweat glands are abundant in the body and essential for thermoregulation. Like mammary glands, they originate from epidermal progenitors. However, they display few signs of cellular turnover, and whether they have stem cells and tissue-regenerative capacity remains largely unexplored. Using lineage tracing, we here identify in sweat ducts multipotent progenitors that transition to unipotency after developing the sweat gland. In characterizing four adult stem cell populations of glandular skin, we show that they display distinct regenerative capabilities and remain unipotent when healing epidermal, myoepithelial-specific, and lumenal-specific injuries. We devise purification schemes and isolate and transcriptionally profile progenitors. Exploiting molecular differences between sweat and mammary glands, we show that only some progenitors regain multipotency to produce de novo ductal and glandular structures, but that these can retain their identity even within certain foreign microenvironments. Our findings provide insight into glandular stem cells and a framework for the further study of sweat gland biology.

INTRODUCTION

Failure to regulate body temperature in hot climates or during exercise can lead to hyperthermia, stroke, and death. Eccrine sweat glands perform this vital function. In response to thermal (trunk skin) and/or emotional stimuli (palmoplantar skin), they produce and secrete salt-enriched sweat fluids (water, sodium, potassium, chloride, urea, lactate, and creatine) into small lumenal orifices that extend to the skin surface (Lobitz and Dobson, 1961). Reaching densities of 200–700/cm^2 of skin surface, they are by far the most abundant glandular structures of the human body (Sato, 1993). In mice, sweat glands are restricted to foot pads, and much of what is known about them stems from observations on human sweat gland morphogenesis and from limited parallels drawn with their distant mammary gland relatives.

In mouse, sweat buds emerge just before birth (embryonic day [E] 17.5), whereas mammary buds appear at E13.5. Both bud types are initiated by Ectodysplasin-A receptor-mediated signaling and begin as morphologically similar, undifferentiated invaginations from epidermis (Cui and Schlessinger, 2006; Mustonen et al., 2004). However, whereas the nascent mammary duct is relatively short and undergoes elaborate branching morphogenesis during development, sweat buds generate a single long duct that extends deep within the dermis.

As the straight duct matures, it forms a coiled gland from its tip (Figure 1A). Like the mammary gland, the secretory coil consists of an outer basal layer of keratin 5 and 14 (K5/K14)$^+$, smooth muscle actin (SMA)$^+$ myoepithelial cells, and an inner suprabasal layer of K8/K18/K19$^+$ lumenal cells (Langbein et al., 2005; Moll and Moll, 1992; Schön et al., 1999). However, the coiled architecture of the sweat gland is highly divergent from the lobular structure of the mammary gland. Additionally, sweat glands have small lumens and show little or no signs of homeostatic change, whereas mammary glands have large lumens and undergo dramatic tissue expansion during pregnancy (Richert et al., 2000). These natural differences in cellular proliferation and turnover may also explain why cancers are so rare in sweat glands but frequent in mammary tissue.

Proliferation and tissue generation are features fueled by adult stem cells. Given the enormous tissue-regenerative capabilities of the mammary gland, it is not surprising that their glandular stem cells have been a long-standing topic of intense study and are now well-characterized. As suggested by earlier studies (Kordon and Smith, 1998) and then documented with purified (K14$^+$α6-integrin^{hi}CD24$^+$) cells, individual myoepithelial progenitors can reconstitute functional mammary glands when introduced into a cleared fat pad (Shackleton et al., 2006; Stingl

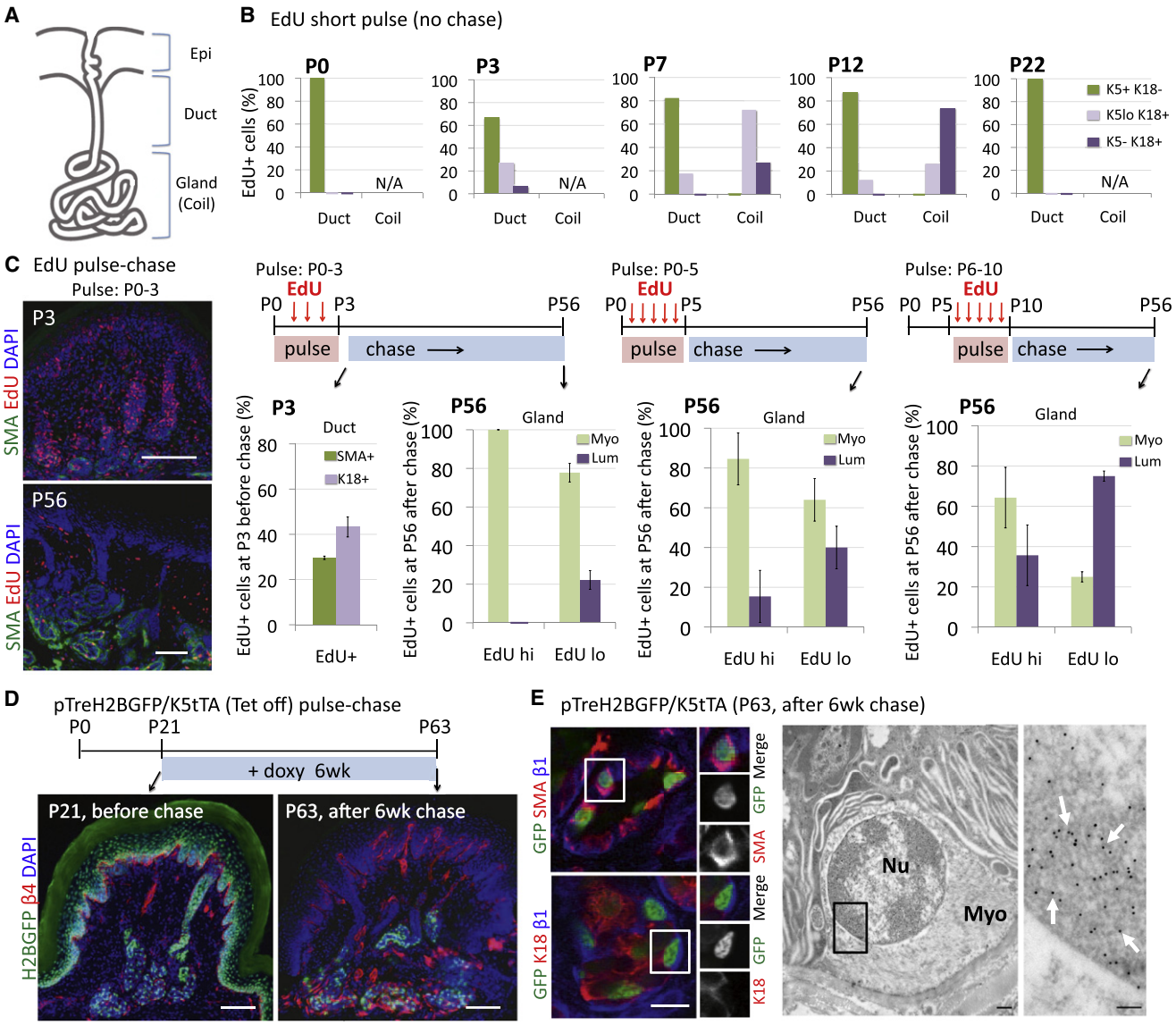

Figure 1. Dramatic Changes in Proliferation Occur within Developing Pawskin during Sweat Gland Morphogenesis

(A) Diagram showing orifice and intraepidermal portion of a sweat duct, which extends from epidermis (Epi) into dermis and terminates in a coiled, secretory gland.

(B) Mice constitutively expressing H2BGFP in *K5 promoter*-active skin epithelium were injected with EdU 4 hr prior to analyses at postnatal ages indicated. EdU^+ (S phase) cells were classified according to keratin and location (within ducts or glands) (n = 100–250 EdU^+ cells from 2–3 mice/stage). Overall gland but not ductal proliferation waned by maturity (P22).

(C) EdU was injected daily for times indicated. Paw pads were analyzed following the last EdU injection and again at P56. Quantifications of EdU label show % myoepithelial (SMA^+) and lumenal ($K18^+$) cells in EdU^{hi} and EdU^{lo} populations (n = 3 mice, > 40 pads). Representative immunofluorescence images for pulse P0→P3 pawskin are shown on the left. Note: label-retaining cells were confined to glands. Scale bars, 50 μm.

(D and E) H2BGFP, expressed in $K5^+$ cells since embryogenesis, was silenced by doxy in Tet-off *pTreH2BGFP/K5tTA* mice as shown. (D) H2BGFP retention occurred only in glands. Scale bar, 50 μm. (E) (Left) Confocal images. Note H2BGFP label retention in SMA^+ but not $K18^+$ sweat gland cells (split channels are for boxed areas). Scale bars, 10 μm. (Right) Ultrathin sections of GFP immunogold-labeled pawskin. Boxed area is magnified to see that myoepithelial cells were labeled (white arrows). Nu, nucleus. Myo, myoepithelial cells. White arrows indicate positive immunogold labeling. Scale bars, 1 μm.

et al., 2006). Based upon these results, it seemed likely that myoepithelial stem cells might give rise to lumenal cells within the mammary gland. However, recent lineage tracings show that during puberty and homeostasis, expansion and maintenance of the mammary gland are fueled largely if not solely by unipotent lumenal and myoepithelial progenitors (Van Keymeulen et al., 2011). The experimental basis for this discrepancy is unknown. It has been speculated that the purified myoepithelial transplantation assays may reflect a wound healing state that does not occur in normal homeostasis.

For the sweat gland, the paucity of massive hormonally induced fluctuations in tissue production raises the question as to whether sweat stem cells exist at all and, if they do, where they are and how they behave in morphogenesis, homeostasis, and wound repair. Moreover, the prominence of the straight duct in this epidermal appendage adds an additional level of complexity that has been largely ignored in the mammary stem cell field.

Much of what is known about proliferative potential within the sweat duct and gland comes from histological studies dating back to the early 1950s. When researchers performed deep dermal injury to the backskin of adult human volunteers, signs of regenerative activity were observed in the damaged glands. In initial experiments, injury-provoked mitoses seemed largely confined to basal cells of the straight duct (Lobitz et al., 1954). However, in subsequent experiments, occasional mitoses were observed in several morphologically distinct epithelial cells residing within closer proximity to the secretory coils, prompting speculation that perhaps these cells might be able to dedifferentiate to repair sweat glands, ducts, and epidermis (Lobitz et al., 1956).

Despite the tantalizing aspects of this hypothesis put forth so long ago, only a few follow-up reports in the past 55 years substantiate regenerative potential for sweat gland cells. Several of these were documented proliferation of dissociated sweat gland cells in culture; most of the in vivo studies focused on the contribution of sweat gland cells to epidermal repair after superficial skin injuries (Biedermann et al., 2010; Miller et al., 1998). However, the precise cells involved were not identified in these studies, nor was the overall regenerative capacity of the sweat gland explored.

Because mammary gland stem cells are the only glandular stem cells studied in detail, it remains unknown to what extent their features might establish a paradigm for glandular stem cells. Similarly, until other glandular stem cells are isolated and profiled, it remains unresolved whether stem cells from different adult glands are analogous and merely differentiate distinctly in response to unique microenvironments or whether defining molecular characteristics are established during morphogenesis. Given the paucity of knowledge about the most abundant gland of our body and the observation that sweat glands are much less dynamic than mammary glands, we've now used the sweat gland as a model to address these key questions in glandular stem cell biology. In addition, we also explore the constituents of the adult sweat duct and test for their stemness.

Here, we report the identification, characterization, and regenerative potential of three types of adult progenitors within the sweat gland and its duct. Remarkably, each of these three populations responds distinctly to different types of skin injuries and to engraftments in a variety of foreign environments. Our findings provide concepts in glandular stem cell biology and reveal fundamental differences in the homeostatic dynamics and the molecular biology of stem cell lineages of glandular and ductal tissues and of other types of epidermal appendages. By illuminating how sweat glands form, are maintained, and differ from mammary glands and hair follicles (HFs), we provide a framework for understanding the roots of some genetic disorders in which sweat glands, and not other epidermal appendages, are specifically affected.

RESULTS

Sweat Gland Development: Emergence of the Straight Duct and Secretory Coil

To gain insights into how the sweat duct and gland develop, we began by monitoring proliferative activity by administering a short pulse (4 hr) of nucleotide analog ethynyldeoxyuridine (EdU) just prior to analysis. We used mice that express histone H2B-green fluorescent protein (H2BGFP) in all K5-expressing cells and analyzed EdU incorporation in pawskin during postnatal development. Because the *K5* promoter is silenced as basal progenitors differentiate, we used fluorescence intensity as a predictor of potential precursor-product relation between basal and suprabasal populations.

Representative immunofluorescence images and quantifications of the data are provided in Figures S1A (available online) and 1B. At postnatal day (P) 0, emerging sweat buds were uniformly GFP^{hi} (K5-expressing). By P3, each bud had grown downward, producing a nascent straight duct. The developing duct was bilayered, with a $K5^{+}$ GFP^{hi} basal layer and a $K5^{lo}$ GFP^{dim} suprabasal layer. Suprabasal cells within the lower nascent duct also expressed K18 and accounted for ~30% of all EdU^{+} cells at this stage.

Ductal proliferation and K18 expression were accompanied by the emergence of a nascent sweat gland from the tip (Figure S1A). $K5^{+}/K18^{-}$ basal cells within developing glands were distinguished from their ductal counterparts by SMA expression and a paucity of EdU^{+} cells. By contrast, whether from the lower duct or the gland, $K18^{+}$ cells still incorporated EdU over a 2 week developmental window. Once mature, proliferation was largely if not solely confined to $K5^{+}/K18^{-}$ basal cells of the sweat duct and was not detected in the sweat gland (Figure 1B, P22). Moreover, whether in the sweat duct or gland, cells were either $K5^{+}$ or $K18^{+}$ at this stage, underscoring the transient nature of double-positive, proliferative suprabasal progenitors during morphogenesis. These results also highlighted early molecular and architectural similarities between proliferative tips of sweat ducts and emerging glands.

Emergence of Infrequently Cycling Myoepithelial Cells during Early Grand Development

To further evaluate cycling behavior within developing sweat ducts and glands, we conducted a series of pulse-chase experiments (Figure 1C). In the first experiment, EdU was administered from P0→P3 to mark proliferating nascent ductal cells and then analyzed at P3 and after 8 weeks of chase. Whether EdU^{hi} or EdU^{lo}, label-retaining cells (LRCs) were found exclusively within mature coiled secretory sweat glands and not straight ducts. Moreover, the majority of EdU^{hi} and ~80% of Edu^{lo} cells were myoepithelial. With EdU labelings of P0→P5, and P6→P10, more lumenal LRCs were detected (Figures 1C and S1B). That said, even at P6→P10, some myoepithelial LRCs were still seen, even though any that had formed by this time were not themselves proliferating (see Figure 1B).

To further explore relative proliferation rates within ductal and glandular populations, we turned to *pTREH2BGFP*/K5tTA (Tet-off) mice (Tumbar et al., 2004). This more sensitive method enabled us to express H2BGFP in all $K5^+$ cells beginning in the embryo and then silence *H2BGFP* transcription by administering doxycycline. At P21, all $K5^+$ basal cells from untreated pawskin epidermis, ducts, and sweat glands were marked by H2BGFP, but after 6 weeks, fluorescence was only retained within sweat gland coils (Figure 1D). Immunofluorescence and immunoelectron microscopy confirmed the myoepithelial identity of these H2BGFP-LRCs (Figure 1E). Together, our collective pulse and pulse-chase studies support the view that cells within the developing lumenal compartment undergo several more rounds of proliferation than myoepithelial cells, but that the entire sweat gland is largely static once it reaches maturity. By contrast, adult basal cells of the sweat duct remain proliferative.

Emergence of Multiple Progenitor Populations during Pawskin Development: Multipotency Versus Unipotency

To test progenitor potential of cells within epidermis, sweat ducts, and glands in vivo, we employed lineage tracing with *RosaLacZ* or *RosaYFP* reporter mice, in which a stop codon excisable by Cre-recombinase exists between a ubiquitously expressed *Rosa26* promoter and the reporter gene. We mated these lines with transgenic strains driving constitutive or inducible expression of Cre-recombinase in distinct cell populations.

To assess the contribution of K5/K14-derived embryonic skin basal cells to sweat gland development, we used *K14Cre* mice and induced β-galactosidase in $K14^+$ cells at E13.5–E15.5 (Vasioukhin et al., 1999). Similar to previous findings on HFs (Vasioukhin et al., 1999) and mammary glands (Van Keymeulen et al., 2011), this tracing established that sweat duct and gland develop from K5/K14-expressing multipotent basal progenitors (Figure 2A).

We shifted to *K14rtta*/*TetO* and *K5CreER* mice, which enabled us to induce RosaYFP in basal cells just after birth, when sweat buds are initiating. Four weeks after induction, two patterns of YFP-marked sweat glands were found: one had only YFP^+ myoepithelial cells; the other displayed YFP in both lumenal and myoepithelial compartments. This was true for both of these Cre drivers (Figures 2B). One possibility consistent with these results is that multipotent K5/$K14^+$ progenitors initiate sweat gland morphogenesis, but as development proceeds, the basal lineage becomes largely unipotent. We tested this directly by analyzing myoepithelial cells in mature sweat glands. When activated at P28→P30, both K5 and K14 Cre drivers selectively marked myoepithelial cells, and after 8–12 weeks of chase, no signs of YFP^+ lumenal cells were detected (Figures 2B and S2C).

The existence of multipotent and unipotent basal progenitors led us to wonder whether there might be equivalent types of suprabasal progenitors, or whether they derive solely from basal progenitors, analogous to what happens in skin epidermis. In searching for additional Cre drivers that might allow us to resolve this issue, we discovered that *Sox9CreER* (Krahl and Sellheyer, 2010) is first activatable within suprabasal nascent ductal cells. Moreover, when induced from P1→P3 and examined at P6, signs of clonal expansion were evident (Figure 2C, *RosaLacZ*). Immunofluorescence microscopy of *RosaYFP* lineage-traced cells confirmed their suprabasal location within nascent ducts. These β1-integrin$^-$, $K18^+$ cells were also weakly positive for K14, in agreement with the temporal appearance of proliferative double-positive progenitors at this site. By P22, progeny of *Sox9CreER*-induced cells were found throughout sweat glands, straight ducts, and even sweat duct orifices. Within the gland, marked progeny were predominately lumenal ($K18^+$), although occasional SMA^+ myoepithelial cells were marked (Figure 2C, *RosaYFP*).

To explore the potential of suprabasal progenitors, we conducted lineage tracings in *K19CreER* and *K18CreER* × *RosaYFP* mice. At P28, YFP-marked lumenal cells were prevalent (Figure 2D). Myoepithelial cells were negative for YFP, and this did not change after 8–12 weeks of chase (Figures S1D and S1E). These findings suggested that *K19* and *K18* promoters had been activated selectively in unipotent lumenal progenitors.

We confirmed the existence of unipotent lumenal progenitors by using *K15CrePGR* mice, whose Cre is inducible by the progesterone analog RU486 (Morris et al., 2004; Langbein et al., 2005). In pawskin, *K15* promoter activity was not detectable until P5, and it was restricted to lumenal cells of emerging secretory coils (Figure 2E). When lineage traced to P22, signs of clonal expansion were apparent, but again, only lumenal cells were marked. The lineage-restricted unipotent behavior of these glandular progenitors was confirmed by fluorescence-activated cell sorting (FACS) analyses (introduced later in the text). Similar signs of maturation-associated fate restrictions were seen within sweat ducts, where proliferative activity became restricted to basal cells (Figure S2A). Moreover, given the overall quiescence of the sweat gland, the lack of label retention within adult ductal basal cells (Figures 1C and 1D) appeared to reflect frequent basal to suprabasal turnover within the duct, analogous to what happens in epidermis.

Taken together, our data pointed to the emergence of three distinct types of unipotent progenitors within mature sweat ducts and glands. Our data further showed that these unipotent progenitors all derive from a common multipotent $K14^+$ sweat bud progenitor. This progenitor then generates a nascent duct replete with distinct $K14^+$ basal and K18/K14 double-positive suprabasal progenitors, both of which transiently maintain multipotency: they expand within their respective layers during sweat duct maturation, and they also form the sweat gland. At this point, progenitors of gland and duct become restricted in potential.

Adult Sweat Duct but Not Gland Progenitors Contribute to Epidermal Wound Repair

The relatively static state of mature sweat glands led us to wonder whether they have long-lived stem cells. To address this question, we focused on how cells within sweat duct and gland respond to injury. For this study, we used *Sox9CreER*/*RosaLacZ* mice, which when induced in adults activated Cre throughout most of these cells (Figure 3A). Two days after induction, pawskin epidermis was scraped to induce re-epithelialization (t = 0 hr). Within 3 days post-wounding, β-gal^+ cells and/or their progeny appeared within regenerating epidermis

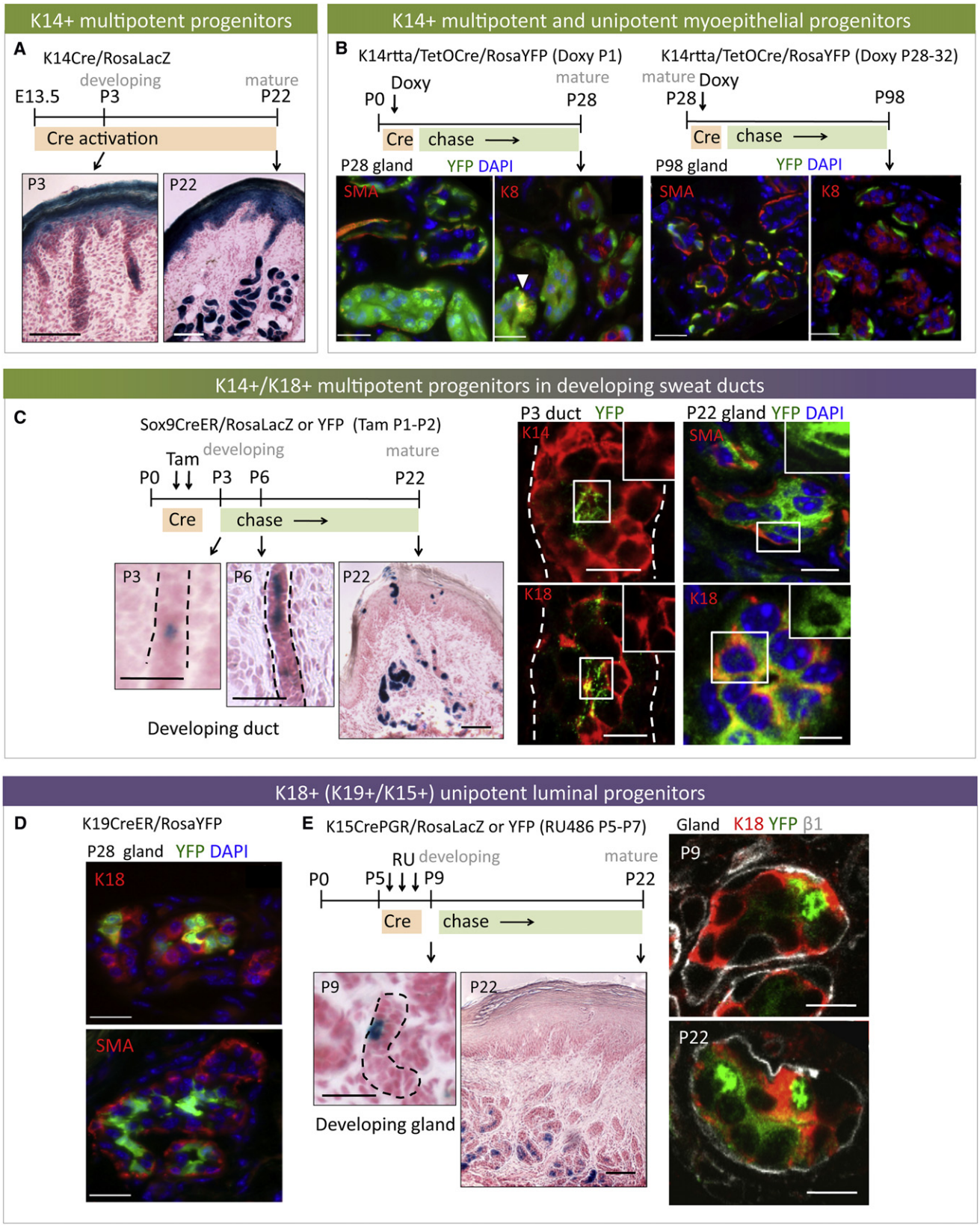
K14+ multipotent progenitors
A
K14Cre/RosaLacZ
developing
mature
E13.5
P3
P22
Cre activation
P3
P22
K14+ multipotent and unipotent myoepithelial progenitors
B
K14rtta/TetOCre/RosaYFP (Doxy P1)
Doxy
P0
mature
P28
Cre
chase
P28 gland
YFP DAPI
SMA
K8
K14rtta/TetOCre/RosaYFP (Doxy P28-32)
mature
Doxy
P28
P98
Cre
chase
P98 gland
YFP DAPI
SMA
K8
K14+/K18+ multipotent progenitors in developing sweat ducts
C
Sox9CreER/RosaLacZ or YFP (Tam P1-P2)
Tam
developing
mature
P0
P3
P6
P22
Cre
chase
P3
P6
P22
Developing duct
P3 duct YFP
K14
K18
P22 gland YFP DAPI
SMA
K18
K18+ (K19+/K15+) unipotent luminal progenitors
D
K19CreER/RosaYFP
P28 gland YFP DAPI
K18
SMA
E
K15CrePGR/RosaLacZ or YFP (RU486 P5-P7)
RU
developing
mature
P0
P5
P9
P22
Cre
chase
P9
P22
Developing gland
Gland K18 YFP β1
P9
P22

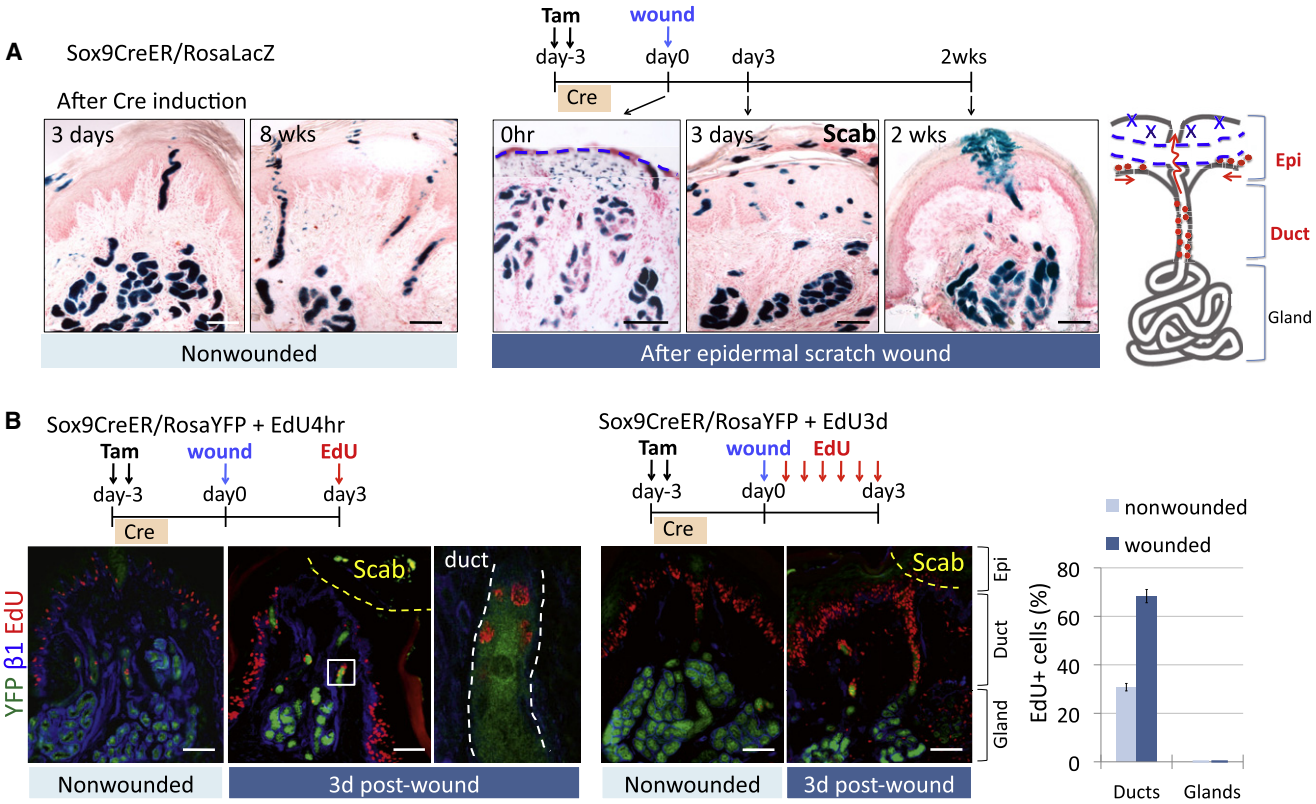

Figure 3. Ductal but Not Glandular Progenitors Participate in Epidermal Wound Repair

(A) Cre was induced in adult *Sox9CreER/RosaLacZ* mice, and pawskins were either examined for LacZ expression 3 days and 8 weeks later (nonwounded, left) or subjected to epidermal scratch wounding and examined at times indicated (wounded, right). Note: In adult mice, Sox9Cre-induction resulted in LacZ expression (blue) in all cellular compartments within the sweat duct and gland. Note expansion of βgal$^+$ intraepidermal cells surrounding the ductal orifice after wounding. Blue dashed lines, removal of epidermis.

(B) Immunofluorescence images of nonwounded and 3 days post-wound pawskin from Cre-induced *Sox9CreER/RosaYFP* mice injected with EdU for 4 hr (left) or 3 days (right) just prior to analysis as indicated. Magnification of boxed area is shown at its right. Quantifications are of EdU$^+$ cells in ducts and glands (n = 2 or 3 mice, > 30 pads). Note that proliferation was restricted to ducts, whereas cells within the sweat gland remained quiescent, as depicted in the diagram in (A). Yellow dashed lines, wounded area covered by a scab. White dashed lines, basement membrane.

All scale bars are 50 μm.

under the scab. By 2 weeks, the narrow column of β-gal$^+$ cells that surrounded sweat duct orifices at t = 0 had broadened considerably (Figure 3A). However, many regenerated cells were unlabeled and hence appeared to come from neighboring epidermis.

To gain further insights, we repeated the assay, this time with a YFP reporter and administering EdU pulses prior to analyses (Figure 3B). As seen by a short (4 hr) EdU pulse (left), pawskin epidermis adjacent to the wound was highly proliferative. Sox9YFP$^+$ ductal cells were also proliferative. In

Figure 2. Multipotent Progenitors in Developing Sweat Ducts Give Rise to Both Lumenal and Myoepithelial Cells in Sweat Glands

(A) Bright-field images of paw pad sections from *K14Cre/RosaLacZ* mice to show emerging (P3) and mature (P22) sweat glands. Sections were stained with X-gal, which turns blue in LacZ$^+$ cells. Counterstaining was done with nuclear fast red.

(B) Immunofluorescence images of mature glands from *K14rtta/TetOCre/RosaYFP* mice induced at P1 and P28 and examined at times indicated. Some glands showed YFP labeling of both myoepithelial (SMA$^+$) and lumenal (K8$^+$) cells (arrow), but others only had YFP$^+$ myoepithelial cells.

(C) Cre was induced at P1→P2 in *Sox9CreER* × *RosaLacZ* or *RosaYFP* mice, and paw pads were analyzed at times indicated. (Left) X-gal-stained bright-field images show that suprabasal nascent ductal cells were *Sox9*-promoter active and contributed to gland formation. (Right) Confocal immunofluorescence. Note: YFP$^+$ nascent ductal cells were double positive for K14/K18. At P22, both myoepithelial and lumenal glandular cells were YFP marked (i.e., ductal-derived). Single channels of boxed areas are shown in insets.

(D) Immunofluorescence images from glands of P28 *K19CreER/RosaYFP* mice Cre-induced at P1. Only lumenal (K18$^+$) cells were YFP marked.

(E) Cre was induced at P5–P7 in *K15CrePGR* × *RosaLacZ* or *RosaYFP* mice, and paw pads were examined at P9 and P22. Note increase over time of YFP$^+$ cells that colabeled with K18, indicative of clonal expansion of marked lumenal cells during gland maturation.

All dashed lines denote basement membrane. All scale bars are 10 μm.

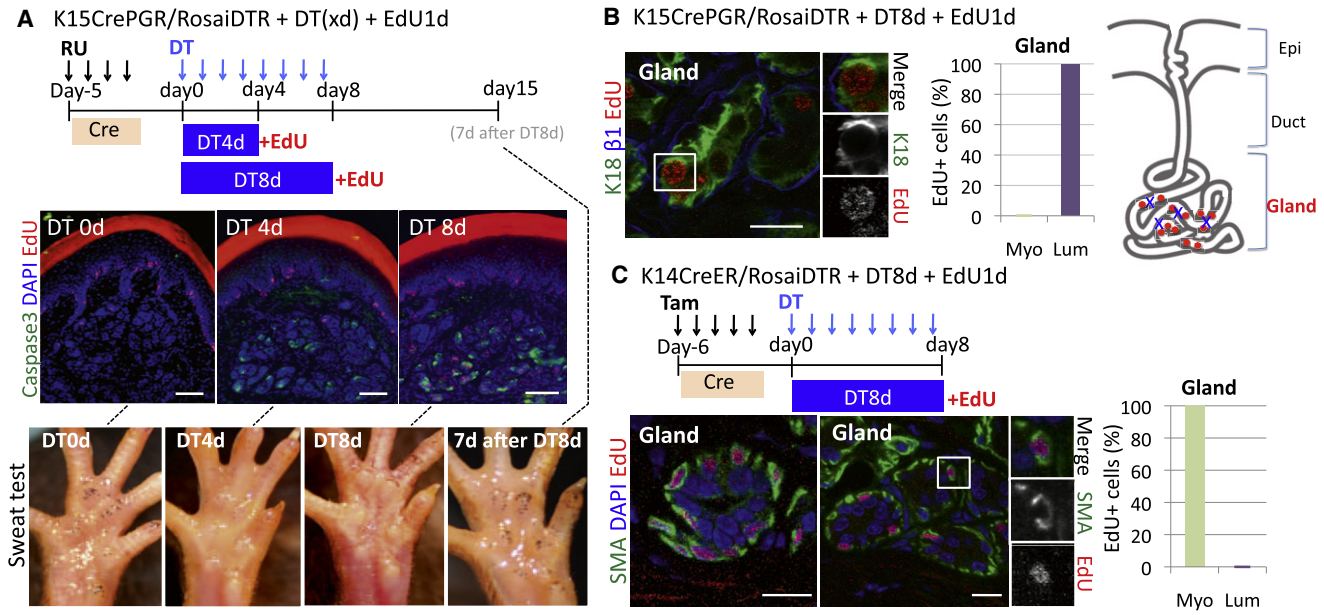

Figure 4. Myoepithelial and Lumenal Progenitors Respond as Unipotent Stem Cells to Glandular Injury

(A and B) Cre was induced in *K15CrePGR/RosaiDTR* mice, which were then treated with DT for times indicated to elicit DTR-mediated lumenal cell death. EdU was given 1 day before immunofluorescence analysis of pawskin, labeled with antibodies as shown (color coding is according to secondary antibodies). (A) Active caspase 3 (apoptosis) occurs only after DT. Scale bars, 50 μm. (Bottom) Sweat tests were performed on paw pads of *K15CrePGR/RosaiDTR* mice before, during, and after DT. Fine black dots reflect functional sweating pores, transiently reduced after glandular injury. (B) Images document lumenal identity of EdU$^+$ cells (split channels for boxed area are at right). Quantifications (n = 2 mice, > 80 EdU$^+$ cells) reveal their selective proliferative response to lumenal cell damage. Scale bar, 10 μm.

(C) Cre was induced in *K14CreER/RosaiDTR* mice, which were then treated with DT for 8 days to induce myoepithelial cell death. EdU was given 1 day before analysis. Representative fluorescence images reveal the myoepithelial identity of EdU$^+$ cells. Quantifications (n = 2 mice, > 120 EdU$^+$ cells) reveal that only myoepithelial cells proliferate in response to myoepithelial apoptosis. Scale bars, 10 μm.

a longer (3 day) pulse, EdU$^+$ ductal cells rose from ~30% to ~70% (right). Sweat glands, however, appeared to remain quiescent throughout wound healing. Their lack of contribution was unambiguously documented with wound studies on *K15CrePGR/RosaLacZ* mice (Figure S3).

Evidence for the Existence of Adult Sweat Gland Stem Cells

We next addressed whether adult sweat gland cells are refractory to wound repair, or whether their regenerative potential is only unleashed when wounds are in closer proximity. To generate more localized tissue damage, we mated *K15CrePGR* and *K14CreER* mice to *RosaiDTR* mice and then induced diphtheria toxin receptor (DTR) expression specifically in either adult lumenal (*K15CrePGR*) or myoepithelial (*K14CreER*) cells. After 4 days of DT, apoptosis (as determined by caspase 3 activation) was selectively induced within a fraction of DTR$^+$ cells (Figure 4A). Few apoptotic cells were detected without DT.

In *K15CrePGR/iDTR* DT-treated mice, myoepithelial cells were spared, not only validating targeting selectivity but also demonstrating that cell death was not a global indirect effect but rather a direct consequence of DT/DTR action on lumenal epithelial cells. As evidenced by EdU pulses given prior to analysis, robust proliferation was induced selectively within K18$^+$ lumenal cells of secretory coils (Figure 4B). Ultrastructural analyses confirmed that apoptotic and mitotic cells were restricted to the lumenal population, whereas neighboring myoepithelial cells remained unaffected (Figure S4). Further reflecting the selective damage were signs of lumen collapse within affected glands.

When similar experiments were performed with *K14CreER/RosaiDTR* mice, the reverse was observed. Although *K14CreER*-mediated targeting of DTR to adult myoepithelial cells was inefficient, it was selective. Moreover, the proliferative response that ensued after DT treatment appeared to be confined to myoepithelial and not lumenal cells (Figure 4C).

To determine whether these proliferative responses were reflective of actual glandular tissue repair, we performed an iodine/starch-based sweat test on paw pads of our animals (Figure 4A, bottom). This procedure detects sweat, reflective of a functional gland. Prior to DT, paws of *K15CrePGR/iDTR* mice responded to the assay by displaying indigo-black dots, indicative of sweat production. After 4 days of DT, indigo dots had decreased in number and intensity, suggesting that sweat production was impaired. Most importantly, 7 days after DT treatment was terminated, dots resurfaced, indicating that sweat gland function had been restored.

Together, these results establish the existence of two distinct types of resident unipotent stem cells. Moreover, both lumenal and myoepithelial stem cells of adult sweat glands possess

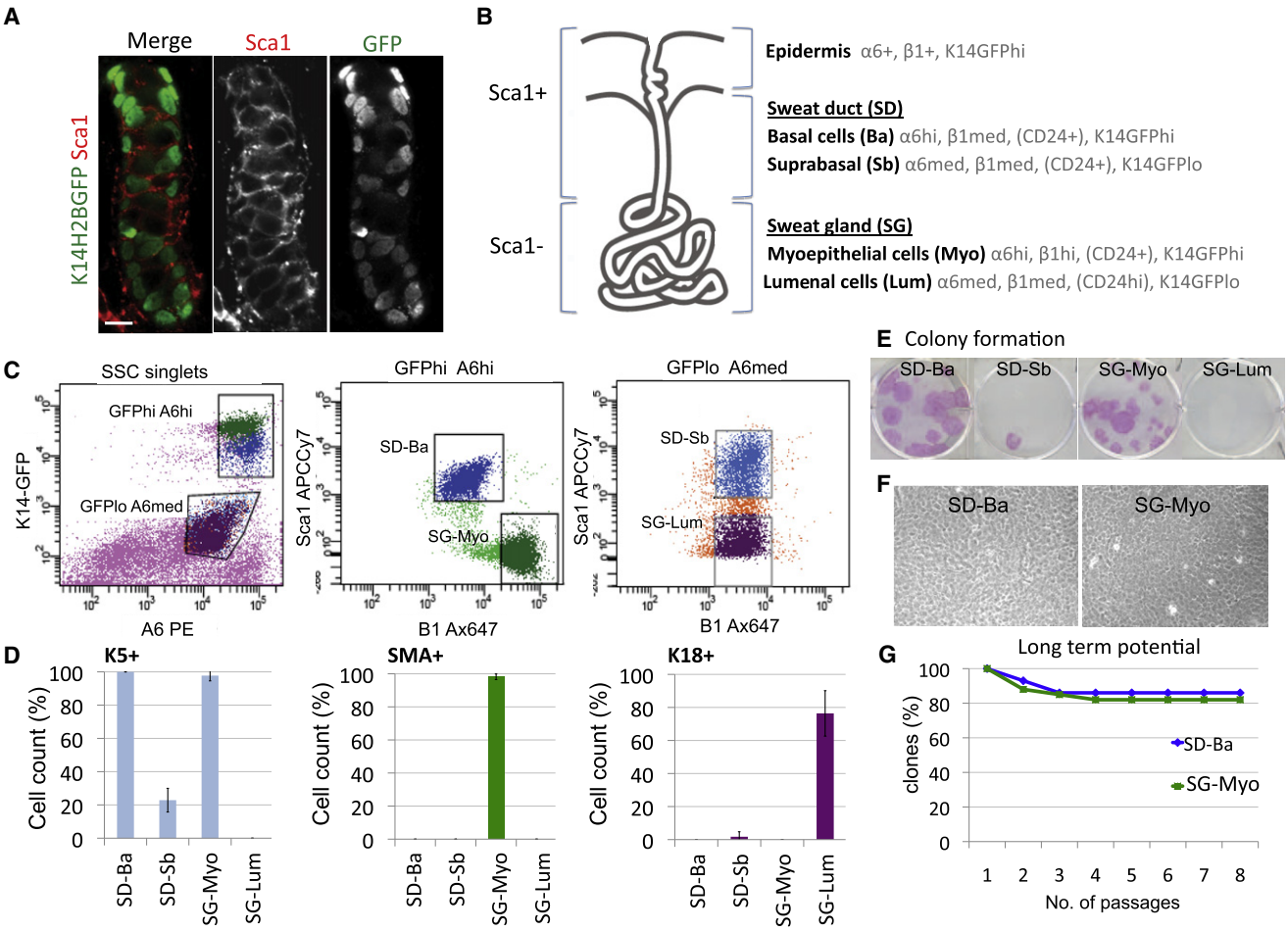

Figure 5. Purification of Distinct Populations from Adult Sweat Ducts and Glands

(A) Image of a sweat duct segment from *K14H2BGFP* pawskin shows that cells are positive for Sca1. Scale bar, 10 μm.

(B) Summary depicting localizations of markers used to isolate different populations from sweat glands and paw pad epidermis. SD, sweat duct. SG, sweat gland.

(C) FACS profiles illustrating the sorting strategy. Ba, basal cells. Sb, suprabasal cells. Myo, myoepithelial cells. Lum, lumenal cells.

(D) Cytospin analyses for different populations isolated from the sweat ducts and glands. Percentages of $K5^+$, SMA^+, and $K18^+$ cells in each population are shown. Quantifications were done with > 150 cells from each of three independent sorts.

(E) Colony formation assay. Representative images of colonies formed from 3,000 FACS-isolated cells after 16 days in culture.

(F) Phase-contrast images of cells within the large holoclones formed from FACS-sorted sweat duct basal cells (SD-Ba, left) and sweat gland myoepithelial cells (SG-Myo, right). Note that both exhibit tightly packed and undifferentiated morphologies.

(G) Long-term potential of purified sweat duct basal cells and sweat gland myoepithelial cells; n = 28 and 34 clones, respectively. Note that for both, > 80% clones survived after eight passages (>3 months) in culture.

regenerative potential that can be tapped in response to localized injury. Progenitor activation was reflected by the enhanced proliferation seen within the gland following injury; regenerative potential was reflected by subsequent restoration of secretory functions following activation and repair.

Purification and Culture of Distinct Progenitor Populations of the Adult Sweat Gland

To delve more deeply into the molecular properties and differences of sweat gland progenitors, we devised methods to purify them. We first showed that (1) similar to the HF infundibulum (Jensen et al., 2008), the sweat duct was marked by Sca1 (Figure 5A); (2) CD29 (β1-integrin) labeled myoepithelial more prominently than straight duct basal cells; (3) CD49f (α6-integrin) labeled all basal populations and to lesser extent suprabasal glandular cells; and (4) analogous to mammary gland lumenal cells (Shackleton et al., 2006; Stingl et al., 2006), CD24 (sialoglycoprotein) strongly labeled sweat gland lumenal cells.

Our purification scheme employed *K14-H2BGFP* transgenic mice in which epidermis, sweat ducts, and glands were brightly fluorescent. After separating pawskin epidermal and dermal (containing sweat ducts and glands) fractions, we used FACS on cells from the dermal fraction to isolate $GFP^{hi}\alpha6^{hi}$ and $GFP^{lo}\alpha6^{med}$ populations, which were further subfractionated to generate straight duct cells (basal: $GFP^{hi}\alpha6^{hi}\beta1^{med}Sca1^{pos}$; suprabasal: $GFP^{lo}\alpha6^{med}\beta1^{med}Sca1^{pos}$) and glandular cells

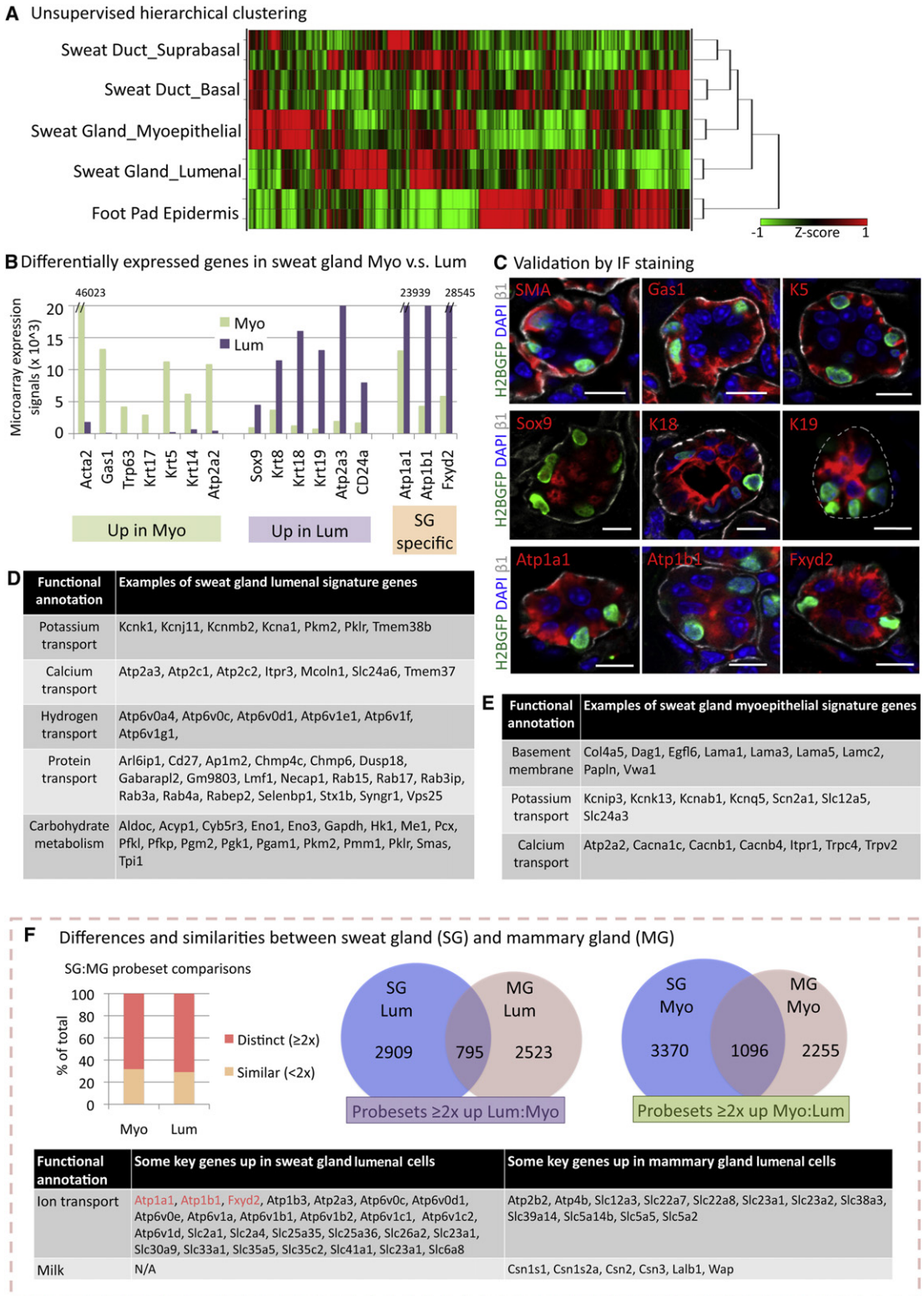

Functional annotation	Examples of sweat gland lumenal signature genes
Potassium transport	Kcnk1, Kcnj11, Kcnmb2, Kcna1, Pkm2, Pklr, Tmem38b
Calcium transport	Atp2a3, Atp2c1, Atp2c2, Itpr3, Mcoln1, Slc24a6, Tmem37
Hydrogen transport	Atp6v0a4, Atp6v0c, Atp6v0d1, Atp6v1e1, Atp6v1f, Atp6v1g1,
Protein transport	Arl6ip1, Cd27, Ap1m2, Chmp4c, Chmp6, Dusp18, Gabarapl2, Gm9803, Lmf1, Necap1, Rab15, Rab17, Rab3ip, Rab3a, Rab4a, Rabep2, Selenbp1, Stx1b, Syngr1, Vps25
Carbohydrate metabolism	Aldoc, Acyp1, Cyb5r3, Eno1, Eno3, Gapdh, Hk1, Me1, Pcx, Pfkl, Pfkp, Pgm2, Pgk1, Pgam1, Pkm2, Pmm1, Pklr, Smas, Tpi1

Functional annotation	Examples of sweat gland myoepithelial signature genes
Basement membrane	Col4a5, Dag1, Egfl6, Lama1, Lama3, Lama5, Lamc2, Papln, Vwa1
Potassium transport	Kcnip3, Kcnk13, Kcnab1, Kcnq5, Scn2a1, Slc12a5, Slc24a3
Calcium transport	Atp2a2, Cacna1c, Cacnb1, Cacnb4, Itpr1, Trpc4, Trpv2

Functional annotation	Some key genes up in sweat gland lumenal cells	Some key genes up in mammary gland lumenal cells
Ion transport	Atp1a1, Atp1b1, Fxyd2, Atp1b3, Atp2a3, Atp6v0c, Atp6v0d1, Atp6v0e, Atp6v1a, Atp6v1b1, Atp6v1b2, Atp6v1c1, Atp6v1c2, Atp6v1d, Slc2a1, Slc2a4, Slc25a35, Slc25a36, Slc26a2, Slc23a1, Slc30a9, Slc33a1, Slc35a5, Slc35c2, Slc41a1, Slc23a1, Slc6a8	Atp2b2, Atp4b, Slc12a3, Slc22a7, Slc22a8, Slc23a1, Slc23a2, Slc38a3, Slc39a14, Slc5a14b, Slc5a5, Slc5a2
Milk	N/A	Csn1s1, Csn1s2a, Csn2, Csn3, Lalb1, Wap

Figure 6. Expression Profiling of Adult Sweat Duct/Gland Populations

(A) Unsupervised Ward clustering and hierarchical analysis of the microarray profiles.

(B) Examples of differentially expressed genes in myoepithelial cells and lumenal cells of the sweat gland. These genes are grouped into three categories: (left) upregulated in myoepithelial cells; (middle) upregulated in lumenal cells; (right) sweat gland specific, compared to mammary gland (see below).

(myoepithelial: GFP$^{hi}\alpha6^{hi}\beta1^{hi}$Sca1^{neg}; lumenal GFP$^{lo}\alpha6^{med}\beta1^{med}$Sca1^{neg}) (Figures 5B and 5C). We validated the sorting strategy by applying it to several transgenic lines expressing GFP or YFP in selective glandular compartments, which enabled us to match FACS with immunofluorescence (Figure S5). The identity and dramatic enrichment of our purified populations was further revealed by cytospin analysis (Figure 5D).

Interestingly, both myoepithelial cells and basal straight duct populations were enriched (1/200–1/750) for cells forming large colonies (holoclones) (Figures 5E–5G). Cells within these colonies were small, tightly packed, and morphologically uniform, with little or no signs of terminal differentiation. Moreover, many colonies could be passaged long term. Notably, these are established features of epidermal and HF stem cells (Barrandon and Green, 1987; Blanpain et al., 2004). By contrast, suprabasal cells from gland and duct failed to grow. This could be due to either the particular culture conditions used or a difference in stemness. We return to this issue later.

Molecular Differences between Sweat Ducts, Sweat Glands, and Mammary Glands

Equipped with the ability to purify adult pawskin sweat duct and gland progenitors and GFP$^{hi}\alpha6^{hi}\beta1^{hi}$Sca1^{pos} basal epidermal cells, we turned to transcriptionally profiling each population to dissect their distinguishing features. Purifications and microarray hybridizations (Affymetrix Mouse430A_2) were performed in duplicate.

Principal component analysis demonstrated that duplicate data sets nicely clustered (data not shown). The relation of each cell population to the others was revealed by unsupervised hierarchical clustering algorithms. As shown by heatmap (Figure 6A), straight duct basal cells were most similar to their suprabasal counterparts but differed markedly from glandular cells. Surprisingly, their most distant relation was pawskin epidermal cells.

Most intriguing were sweat gland features, where > 400 genes scored as being upregulated by $\geq$ 2× in one compartment over the other. Other genes were upregulated specifically in either lumenal or myoepithelial relative to sweat duct or pawskin epidermis. Myoepithelial and lumenal signatures were generated as messenger RNAs (mRNAs) upregulated by $\geq$ 2× relative to all other epithelial populations (Table S1). Besides proteins previously affiliated with sweat glands (Cui et al., 2012; Sato and Sato, 2000; Schön et al., 1999; Song et al., 2002; and references therein), our data revealed a new array of genes (Figure 6B and Table S1). Representative expression-based validations are shown in Figure 6C.

Several functional annotations (grouped according to DAVID) featured prominently within the lumenal signature (Figure 6D). Most notable were mRNAs encoding proteins involved in ion transport, such as Na^+/K^+ and/or Ca^{2+}-ATPases. The lumenal signature also featured transport-related categories, e.g., hydrogen and protein transport, that were not seen in the myoepithelial signature (compare Figures 6D and 6E). Another distinction was the preponderance of lumenal genes involved in carbohydrate metabolism, a link made previously from pharmacologic studies (Sato and Dobson, 1973). More extensive lists for myoepithelial and lumenal signature genes are shown in Table S1.

Given the structural similarities of mammary and sweat glands, we sought to compare our gene expression profiles with those published for mammary glands (Shackleton et al., 2006; Stingl et al., 2006). Although inherent caveats are imposed by differences in purification schemes and transcriptional profiling platforms, the comparisons were nevertheless revealing (Figure 6F and Table S2). Whether myoepithelial or lumenal, the overlap in molecular signatures of mammary and sweat gland counterparts was surprisingly modest. For myoepithelia, shared functional annotations included genes involved in smooth muscle contraction, cell adhesion/basement membrane, and TGF-β, Wnt, and hedgehog signaling pathways (see also Kunisada et al., 2009). For lumenal epithelia, this included cytoskeletal, metabolic, and Notch pathway genes. These parallels aside, sweat and mammary signatures were otherwise strikingly divergent. Among notable lumenal differences were mRNAs encoding ion transport proteins (preferentially expressed by sweat glands) and milk proteins (preferentially expressed by mammary glands).

Adult Myoepithelial and Sweat Duct Progenitors Can Regenerate De Novo Sweat Glands in Some but Not All Foreign Microenvironments

We next asked whether foreign microenvironments might influence the identity and unipotency of adult sweat gland progenitors. To examine these issues, we challenged the sweat gland progenitors to make tissue de novo by transplanting them into different body sites. Although kidney capsule implantations were not consistent and paw pads posed technical impracticalities, three distinct body locations were informative: mammary fat pads, shoulder fat pads, and backskin.

In the first experiment, we purified K14-H2BGFP-marked myoepithelial cells and transplanted them into the cleared mammary fat pads of virgin female *Nu/Nu* mice. Within 8 weeks, de novo green fluorescent glandular structures appeared (Figure 7A). Notably, K14-H2BGFP$^+$ cells were SMA$^+$ and oriented their integrin$^+$ basal surface toward the gland periphery. Within the gland were K18$^+$/K14$^-$ cells, many of which were suprabasal. Although lumens were small, their existence offered further

(C) Immunofluorescence microscopy to validate expression of sweat gland proteins whose RNA expression is upregulated in either myoepithelial or lumenal cells or both. Sections are from K14H2BGFP adult pawskin. GFP marks myoepithelial cell nuclei. Dashed line, basement membrane. Scale bars, 10 μm.
(D) Functional annotations of some of the genes upregulated $\geq$ 2× in sweat gland lumenal cells.
(E) Functional annotations of some of the genes upregulated $\geq$ 2× in sweat gland myoepithelial cells.
(F) Comparisons of sweat and mammary gland mRNA profiles. Graph at left shows percentage of total probesets that are similar (<2×) or distinct ($\geq$2×) in arrays from myoepithelial cells and lumenal cells of sweat and mammary glands. Venn diagrams showing marked differences between the sweat and mammary gland molecular signatures (genes upregulated $\geq$ 2×) of both lumenal (left) and myoepithelial (right) cells. Table highlights several of the key differentially expressed genes in lumenal cells of sweat and mammary glands, respectively.

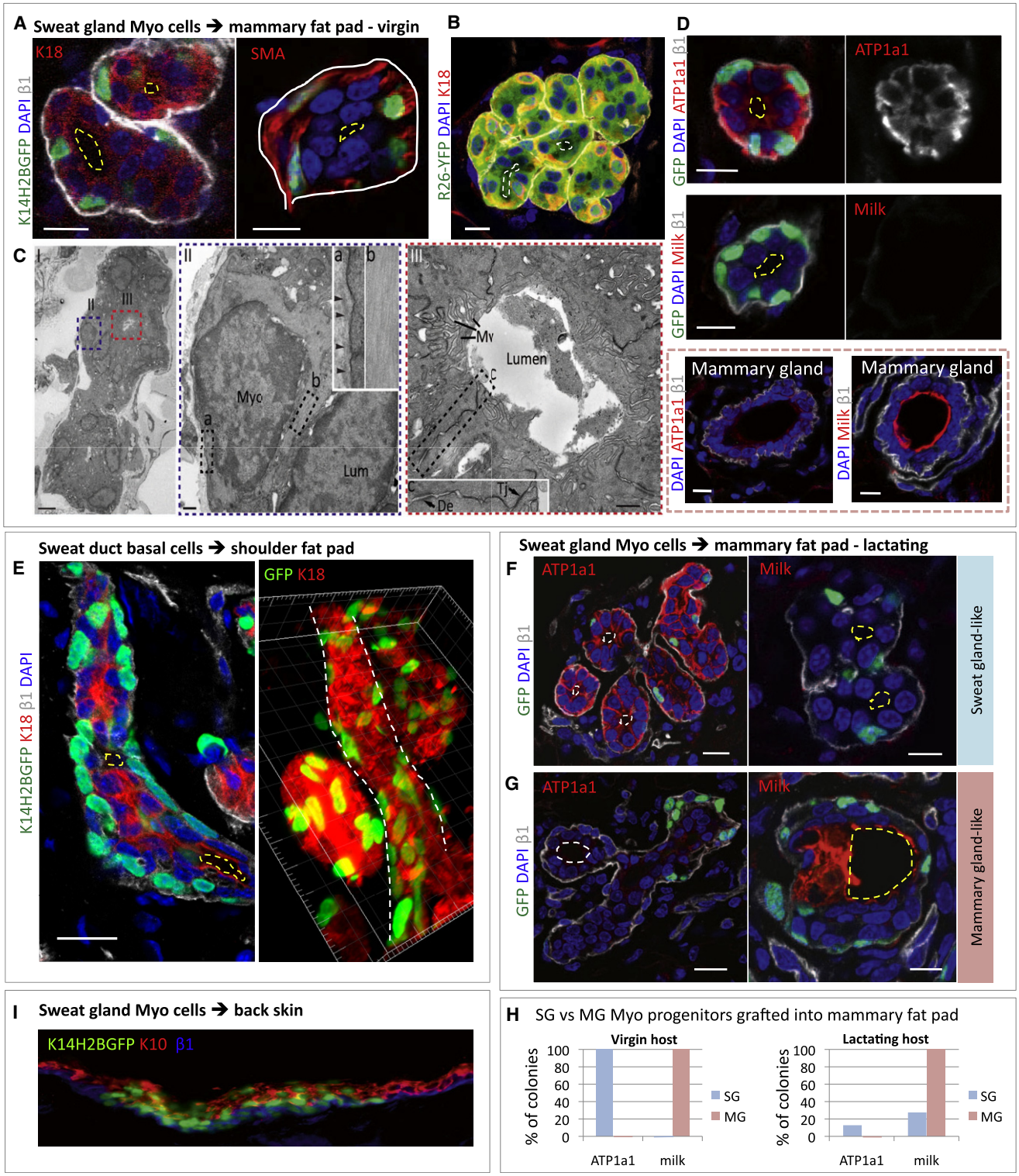

Figure 7. Purified Progenitors from Sweat Ducts and Glands Exhibit De Novo Tissue Morphogenesis and Maintain Their Identity when Engrafted into Some but Not All Foreign Microenvironments

(A) Sweat gland myoepithelial cells from K14H2BGFP mice were FACS purified and transplanted into mammary fat pads of virgin *Nu/Nu* mice. Engrafted tissues were analyzed at 10 weeks. K18, β1, and SMA immunolabelings of sections of K14H2BGFP gland-like structures reveal polarized architecture. Yellow dashed lines outline lumens. Scale bars, 10 μm.

signs of a polarized glandular structure. When administered during the regenerative process, EdU incorporated predominantly into K18$^+$ cells, suggesting that the lumenal compartment of these glands was still expanding at the time of analyses (Figure S6A).

Because *K14-H2BGFP* is silenced in lumenal cells, we repeated the transplantation experiments with FACS-purified myoepithelial cells from *K14Cre/RosaYFP* mice (Figure 7B). The presence of YFP$^+$/K18$^+$ cells indicated that de novo glandular morphogenesis was driven by our FACS-purified RosaYFP$^+$ donor cells and not a mixture of donor and host epithelial cells. De novo glands persisted for 4 months (the furthest time point we took), reflective of an ability to survive long term in this foreign environment.

Ultrastructural analyses of de novo structures revealed classical glandular features (Figure 7C). An underlying basement membrane encased the well-polarized myoepithelial cells replete with bundles of actin filaments reflective of a rich actomyosin cytoskeleton. Inner lumenal cells were also highly polarized. Desmosomes and adherens junctions denoted sealed intercellular membranes, culminating in tight junctions at the lumen boundary. By contrast, apical lumenal surfaces were replete with microvilli (Mv), and lumens were small. As visualized by assembling z stacks of confocal images of thick tissue sections, de novo glands were coiled, and a continuous narrow lumen extended through the various coiled regions of the gland (Figure S6B and not shown).

To investigate glandular identity in further detail, we exploited our comparative gene expression data. Antibodies against sodium/potassium channel protein ATP1a1 labeled de novo K14-H2BGFP glandular structures but not mammary glands. Conversely, antibodies against milk proteins, a hallmark of mammary glands whether lactating or not, labeled only mammary glands and not de novo glands (Figure 7D).

Similar results were obtained when we engrafted sweat duct and gland cells into shoulder fat pads of recipient mice (Figure S6C). Ductal progenitors even showed hints of broader morphogenetic potential, as evidenced by a straight duct-like structure (see Figure 7E). Moreover, as visible in some sections and confirmed by three-dimensional reconstruction, both coiled gland and straight duct-like structures displayed lumen, which were small, as characteristic of sweat glands. Finally, neither mammary nor shoulder pad sites supported glandular growth by our purified lumenal progenitors. Although dissecting the underlying bases for differences in progenitor behaviors ex vivo are beyond the scope of the present study, it is intriguing that these in vivo tests for stemness were in good agreement with those obtained from cell culture.

To further challenge the possible impact of microenvironment on progenitor behavior, we repeated our engraftment experiments, this time in cleared mammary fat pads of lactating mice. As before, de novo tissue structures arose with sweat gland-like features, including a small lumen and ATP1a1 expression (Figure 7F). Interestingly, however, ~20% of de novo glands from sweat gland progenitors displayed an enlarged lumen and branching-like morphogenesis, accompanied by milk protein expression (Figure 7G). Additionally, some glands did not appear to express either ATP1a1 or milk protein, perhaps reflective of a transitory state. Although only partial, this fluctuation in glandular fate was not seen in engraftments into virgin females, nor was it observed in engraftments that we performed with mammary myoepithelial progenitors (Figure 7H). Moreover, as sweat gland progenitors in their native paw pad environment do not show such morphological or fate alterations during pregnancy, the changes appeared to be rooted in a hormonally induced change within the mammary fat pad microenvironment that in turn affected the behavior of the de novo sweat gland-like structures.

A final example of the importance of microenvironment was revealed by transplanting basal sweat duct and gland progenitors to backskin. In this case, we saw no sign of de novo ducts or glands; rather, progenitors produced a stratified epidermis

(B) Image of a 4 month graft of transplanted FACS-purified myoepithelial cells as in (A) but from RosaYFP mice. The entire de novo glandular structure is YFP$^+$, demonstrating that K18$^+$ lumenal cells are derived from the donor sweat gland myoepithelial population and not host mammary cells. Scale bars, 10 μm.

(C) Ultrastructure analysis of de novo glandular structure within host mammary fat pad 10 weeks after transplanting donor K14H2BGFP$^+$ myoepithelial cells. GFP$^+$ glandular structures were identified by correlative immunofluorescence and TEM. I: Example of glandular structure. Cells are organized around an open lumenal space. Boxed areas are enlarged in II and III. Scale bar, 10 μm. II: Myoepithelial cell (Myo) beside a lumenal cell (Lum). Boxed areas are magnified in insets. Boxed area (a), myoepithelial cell attachment to basement membrane (arrowheads). Boxed area (b) shows dense actin filament bundles within myoeptithelial cytoplasm. Scale bar, 500 nm. III: Lumenal cells within gland. Note numerous apical microvilli (Mv). Intercellular junctions are boxed, showing desmosome (De) and tight junction (Tj). Scale bars, 500 nm.

(D) Immunofluorescence for ATP1a1 (sweat gland-specific marker) and milk protein (mammary gland-specific marker) in de novo glandular structures from transplanted FACS-purified K14H2BGFP sweat gland myoepithelial cells and from mammary gland control tissue. Note that sweat gland myoepithelial cells retain their character even when engrafted to a mammary microenvironment. Scale bars, 10 μm.

(E) Purified K14H2BGFP$^+$ sweat duct basal cells were transplanted into mouse shoulder fat pad, and tissue was analyzed 8 weeks later. Left image shows a straight duct-like structure with K18$^+$ suprabasal cells and K14H2BGFP$^+$ basal cells. Yellow dashed lines outline lumens. Right image shows a 3D reconstruction from a z stack. White dashed lines demarcate the straight duct-like structure. Scale bars, 10 μm.

(F and G) Purified K14H2BGFP$^+$ sweat gland myoepithelial cells were transplanted into mammary fat pad of recipient mouse that went through pregnancy after engraftment and was lactating when the graft was taken. (F) Representative images of some sweat gland-like colonies, which still express sweat gland markers and small lumens (yellow dashed lines). Note that some glands show slight branching morphology (left). (G) Representative images of some mammary gland-like colonies that show diminished expression of sweat gland marker (ATP1a1, left) and are positive for milk proteins (right). Note that they exhibit clear branching morphology and enlarged lumens, not seen in grafts from virgin hosts. Scale bars, 10 μm.

(H) Graphs showing differences of sweat gland (SG) and mammary gland (MG) myoepithelial progenitors when FACS-purified from K14H2BGFP$^+$ mice and engrafted into mammary fat pads of virgin and lactating hosts.

(I) Purified K14H2BGFP$^+$ sweat gland myoepithelial cells were combined with dermal fibroblasts and transplanted into mouse back skin. Note epidermal differentiation of engrafted cells.

(Figure 7I). Moreover, the de novo epidermis resembled backskin and not pawskin. Collectively, our transplantation experiments into four distinct microenvironments underscored the existence of both intrinsic and microenvironmental factors that impact the behavior and fate specification of two types of stem cells from sweat ducts and glands.

DISCUSSION

Two Populations of Progenitors in the Nascent Sweat Duct

Our studies provide insights into the most abundant glandular epithelia of the human body and ones that have endowed humans with the remarkable capacity to inhabit extreme climates of a range not possible for animals whose skin cannot sweat. We have found that like the mammary gland (Van Keymeulen et al., 2011), sweat gland development begins as an epidermal bud of multipotent $K14^+$ progenitors. However, as downward growth proceeds, the nascent sweat duct never branches. Moreover, within its lower half, $K14^+$ progenitors stratify to generate a transient but proliferative $K14^{low}/K18^+$ suprabasal layer of progenitors. Much of the morphogenetic potential to form sweat glands appears to stem from these $K14^+$ basal and $K14^{low}/K18^+$ suprabasal ductal progenitors, which give rise to myoepithelial and lumenal cells, respectively, of the sweat gland.

Four Populations of Stem Cells in Adult Pawskin: Multipotency versus Unipotency

Our lineage tracing and EdU pulse-chase studies expanded upon early histological observations (Lobitz et al., 1956) and unveiled the existence of different progenitor populations within glandular skin. In adult pawskin, both sweat ducts and epidermis displayed considerable homeostatic turnover, and each followed distinct basal→suprabasal differentiation programs. Moreover, both ductal and epidermal progenitors participated in epidermal wound repair, although ductal progenitors seemed focused on regenerating the sweat duct orifice, whereas epidermal progenitors adjacent to the wound showed more activity in epidermal repair. In contrast, sweat glands remained quiescent during epidermal wound repair and displayed little if any turnover during normal homeostasis.

The quiescence of sweat glands during normal homeostasis and after epidermal injury posed a challenge not faced for mammary glands. To discern the lineage relation between myoepithelial and lumenal cells and test for stemness, we had to engineer mice and selectively target each sweat gland population for DT-induced cell death. In response, surviving glandular cells proliferated, and sweat production was restored, thereby exposing the glandular cells' regenerative potential. Notably, myoepithelial progenitors only replaced damaged myoepithelial cells in this assay, whereas lumenal progenitors only replaced damaged lumenal cells.

Overall, our findings point to the existence of four resident progenitor populations, each of which supports primarily one lineage within glandular skin. Moreover, of the three $K14^+$ basal progenitors, only two appear to contribute to a stratified program of differentiation.

Intrinsic versus Extrinsic Features of Stemness and Multipotency

Our transplantation studies revealed a diverse array of multipotent regenerative potentials not displayed by adult sweat gland progenitors in their normal tissue context. Previously, it was speculated that similar expanded potential displayed by adult mammary myoepithelia (Shackleton et al., 2006; Stingl et al., 2006) might be reflective of a wound response (Van Keymeulen et al., 2011). However, our studies show that at least for the sweat duct/gland, progenitors remain largely unipotent during wound repair. By contrast, the de novo sweat ducts/glands generated by engraftment paralleled those generated in developmental glandular morphogenesis. Thus, purified adult ductal basal cells gave rise to glands and ducts in rare cases, whereas purified myoepithelial counterparts consistently formed sweat glands. That said, even this analogy is not sufficient to explain why adult myoepithelial progenitors generate a stratified epidermis when engrafted onto backskin. In skin development, such versatility is only exhibited by epidermal precursors of glandular tissue.

In transplantation assays, lumenal cells did not show this diverse behavior. Moreover, in similar transplantation experiments performed with purified adult mammary myoepithelial cells, the frequency of lumenal differentiation declined when the engraftment mixture was spiked with increasing numbers of unmarked lumenal cells (Van Keymeulen et al., 2011). Overall, these findings suggest that even though lumenal progenitors can replenish dying lumenal cells in the context of normal glands, they are not able to support de novo morphogenesis either in normal development or when transplanted.

Insights into Glandular Biology

Despite their temporal lineage ties during morphogenesis, the relation between adult ductal and glandular progenitors has long remained unclear. Our studies now show that many distinguishing features of sweat glands, such as secretory coil-specific sodium/potassium transporter proteins, are not expressed in sweat ducts. Moreover, ductal and glandular progenitors differ not only in normal homeostasis but also in their responses to different types of tissue injury.

Our studies also offer insights into distinctions between resident stem cells of different types of glands. Despite emerging paradigms between stem cells of sweat and mammary glands, their lineages remain molecularly and morphologically distinct. Moreover, the sweat gland-specific signature and morphology appear to some extent to be preprogrammed within adult myoepithelial progenitors. Thus, even when sweat gland myoepithelial progenitors were engrafted into virgin mammary or shoulder fat pad environments, these features persisted within sweat gland structures that formed de novo. The ability of glandular progenitors to faithfully maintain their identity even when placed within foreign microenvironments has hitherto not been recognized and was surprising given prior reports that dissociated testis cells and cultured neural stem cells transdifferentiate into mammary glands when engrafted into cleared mammary pads (Booth et al., 2008; Boulanger et al., 2007).

Our results were also intriguing given the well-documented importance of embryonic mesenchyme in dictating sweat gland

fate (Ferraris et al., 2000). The intrinsic differences displayed by adult mammary and sweat gland stem cells when placed in a common setting suggest that they are established during morphogenesis. In the future, it will be interesting to determine how reciprocal signaling between mesenchyme and epithelium differs spatially and temporally as mammary and sweat glands develop from epidermal precursors.

Given the ability of sweat gland myoepithelial cells to maintain their identity in the mammary fat pads of virgin females, it was intriguing to find that this fluctuated when the same engraftments were carried out in lactating animals. Because pregnancy does not induce milk production in pawskin sweat glands, the lactogenic hormones must specifically alter mammary stroma in a way that overpowers the preprogrammed features of adult glandular stem cells that otherwise govern identity. They further suggest that despite distinguishing features of adult myoepithelial stem cells of different glands, their relation is sufficiently close such that stromal changes may at least influence, if not fully override, their specified glandular behavior. This underscores the value of exploring different stem cells from related tissues and has profound implications for regenerative medicine.

EXPERIMENTAL PROCEDURES

Mouse Manipulations

Unstimulated (no doxy) *pTreH2BGFP* × *K5tTA* (K5-Tet-off) mice were used for experiments in Figure 1B. For experiments in Figures 1D and 1E, H2BGFP was silenced by doxycycline (2 mg/kg). EdU, Cre inductions, and scratch wounding are described in the Extended Experimental Procedures. For sweat tests, an iodine-starch method was used (Blecher, 1986 and references therein): iodine/alcohol solution (2%) was applied to palmar surface of a restrained mouse. After the alcohol evaporated, a suspension of 1 g starch/1 ml castor oil was applied. Fine black dots appeared within 2 min on paw pads and at the toe tips of an actively sweating mouse.

Sweat Gland Cell Preparation and FACS Sorting and Engraftment

Mouse paw pads were collected as biopsies and incubated in 5 mM EDTA, 37°C, for 1 hr. After manual dissection of epidermis, the dermal fraction containing sweat glands was placed in Hanks Balanced Salt Solution (Lonza) with 1000 U/ml collagenase and 300 U/ml hyaluronadase (Sigma) and digested for 1 hr at 37°C. 0.25% trypsin-EDTA (GIBCO) was added for additional digestion for 10 min. Digested tissues were suspended and washed with PBS containing 5% of fetal bovine serum (FBS), then filtered through 40 μm cell strainers to make single-cell suspensions. Samples were labeled with fluorescently conjugated Abs: Sca1-APCCy7 (1:1500, eBioscience), α6-PE (1:1000, eBioscience), β1-Alexa647 (1:500, eBioscience) at 4°C for 15 min and washed with PBS containing 0.1% BSA. DAPI was added for dead cell exclusion. Cell sorting was performed on FACS Aria system with FACS DiVa software (BD Bioscience). Sorted cells were mixed with Matrigel (1:1, BD Biosciences) and injected into cleared mammary or shoulder fat pads of female *Nu/Nu* mice.

ACCESSION NUMBERS

The raw and normalized microarray data will be made available at the Gene Expression Omnibus under number GSE37274 (http://www.ncbi.nlm.nih.gov/geo/).

SUPPLEMENTAL INFORMATION

Supplemental Information includes Extended Experimental Procedures, six figures, and two tables and can be found with this article online at http://dx.doi.org/10.1016/j.cell.2012.04.045.

ACKNOWLEDGMENTS

We thank D. Chu for sparking interest in sweat glands in the Fuchs lab. We thank Y.-C. Hsu, X. Wu, and B. Keyes for intellectual input and helpful suggestions. We thank Rockefeller's Comparative Bioscience Center (AAALAC accredited) for care and breeding of mice in accordance with National Institutes of Health (NIH) guidelines; Bioimaging Center (A. North, director) for advice on image acquisition; and Flow Cytometry facility (S. Mazel, director) for FACS sorting. E.F. is an Investigator of The Howard Hughes Medical Institute. C.P.L. is a Ruth Kirschstein Postdoctoral Fellow (NIH 5F32AR060654-02). This work was supported initially by pilot grants from Stem Cell Research and Starr Foundations (E.F.) and more recently by NIH R01-AR050452 (E.F.).

Received: February 2, 2012
Revised: March 23, 2012
Accepted: April 30, 2012
Published: July 5, 2012

REFERENCES

Barrandon, Y., and Green, H. (1987). Three clonal types of keratinocyte with different capacities for multiplication. Proc. Natl. Acad. Sci. USA *84*, 2302–2306.

Biedermann, T., Pontiggia, L., Böttcher-Haberzeth, S., Tharakan, S., Braziulis, E., Schiestl, C., Meuli, M., and Reichmann, E. (2010). Human eccrine sweat gland cells can reconstitute a stratified epidermis. J. Invest. Dermatol. *130*, 1996–2009.

Blanpain, C., Lowry, W.E., Geoghegan, A., Polak, L., and Fuchs, E. (2004). Self-renewal, multipotency, and the existence of two cell populations within an epithelial stem cell niche. Cell *118*, 635–648.

Blecher, S.R. (1986). Anhidrosis and absence of sweat glands in mice hemizygous for the Tabby gene: supportive evidence for the hypothesis of homology between Tabby and human anhidrotic (hypohidrotic) ectodermal dysplasia (Christ-Siemens-Touraine syndrome). J. Invest. Dermatol. *87*, 720–722.

Booth, B.W., Mack, D.L., Androutsellis-Theotokis, A., McKay, R.D., Boulanger, C.A., and Smith, G.H. (2008). The mammary microenvironment alters the differentiation repertoire of neural stem cells. Proc. Natl. Acad. Sci. USA *105*, 14891–14896.

Boulanger, C.A., Mack, D.L., Booth, B.W., and Smith, G.H. (2007). Interaction with the mammary microenvironment redirects spermatogenic cell fate in vivo. Proc. Natl. Acad. Sci. USA *104*, 3871–3876.

Cui, C.Y., and Schlessinger, D. (2006). EDA signaling and skin appendage development. Cell Cycle *5*, 2477–2483.

Cui, C.Y., Childress, V., Piao, Y., Michel, M., Johnson, A.A., Kunisada, M., Ko, M.S., Kaestner, K.H., Marmorstein, A.D., and Schlessinger, D. (2012). Forkhead transcription factor FoxA1 regulates sweat secretion through Bestrophin 2 anion channel and Na-K-Cl cotransporter 1. Proc. Natl. Acad. Sci. USA *109*, 1199–1203.

Ferraris, C., Chevalier, G., Favier, B., Jahoda, C.A., and Dhouailly, D. (2000). Adult corneal epithelium basal cells possess the capacity to activate epidermal, pilosebaceous and sweat gland genetic programs in response to embryonic dermal stimuli. Development *127*, 5487–5495.

Jensen, U.B., Yan, X., Triel, C., Woo, S.H., Christensen, R., and Owens, D.M. (2008). A distinct population of clonogenic and multipotent murine follicular keratinocytes residing in the upper isthmus. J. Cell Sci. *121*, 609–617.

Kordon, E.C., and Smith, G.H. (1998). An entire functional mammary gland may comprise the progeny from a single cell. Development *125*, 1921–1930.

Krahl, D., and Sellheyer, K. (2010). Sox9, more than a marker of the outer root sheath: spatiotemporal expression pattern during human cutaneous embryogenesis. J. Cutan. Pathol. *37*, 350–356.

Kunisada, M., Cui, C.Y., Piao, Y., Ko, M.S., and Schlessinger, D. (2009). Requirement for Shh and Fox family genes at different stages in sweat gland development. Hum. Mol. Genet. *18*, 1769–1778.

Langbein, L., Rogers, M.A., Praetzel, S., Cribier, B., Peltre, B., Gassler, N., and Schweizer, J. (2005). Characterization of a novel human type II epithelial keratin K1b, specifically expressed in eccrine sweat glands. J. Invest. Dermatol. *125*, 428–444.

Lobitz, W.C., Jr., and Dobson, R.L. (1961). Dermatology: the eccrine sweat glands. Annu. Rev. Med. *12*, 289–298.

Lobitz, W.C., Jr., Holyoke, J.B., and Montagna, W. (1954). Responses of the human eccrine sweat duct to controlled injury: growth center of the epidermal sweat duct unit. J. Invest. Dermatol. *23*, 329–344.

Lobitz, W.C., Jr., Holyoke, J.B., and Brophy, D. (1956). Response of the human eccrine sweat duct to dermal injury. J. Invest. Dermatol. *26*, 247–259, discussion, 259–262.

Miller, S.J., Burke, E.M., Rader, M.D., Coulombe, P.A., and Lavker, R.M. (1998). Re-epithelialization of porcine skin by the sweat apparatus. J. Invest. Dermatol. *110*, 13–19.

Moll, I., and Moll, R. (1992). Changes of expression of intermediate filament proteins during ontogenesis of eccrine sweat glands. J. Invest. Dermatol. *98*, 777–785.

Morris, R.J., Liu, Y., Marles, L., Yang, Z., Trempus, C., Li, S., Lin, J.S., Sawicki, J.A., and Cotsarelis, G. (2004). Capturing and profiling adult hair follicle stem cells. Nat. Biotechnol. *22*, 411–417.

Mustonen, T., Ilmonen, M., Pummila, M., Kangas, A.T., Laurikkala, J., Jaatinen, R., Pispa, J., Gaide, O., Schneider, P., Thesleff, I., and Mikkola, M.L. (2004). Ectodysplasin A1 promotes placodal cell fate during early morphogenesis of ectodermal appendages. Development *131*, 4907–4919.

Richert, M.M., Schwertfeger, K.L., Ryder, J.W., and Anderson, S.M. (2000). An atlas of mouse mammary gland development. J. Mammary Gland Biol. Neoplasia *5*, 227–241.

Sato, K. (1993). Biology of the eccrine sweat gland. In Dermatology in Medicine, T.B. Fitzpatrick, A.Z. Eisen, K. Wolff, I.M. Freedberg, and K.F. Austen, eds. (New York: McGraw-Hill), pp. 221–241.

Sato, K., and Dobson, R.L. (1973). Glucose metabolism of the isolated eccrine sweat gland. II. The relation between glucose metabolism and sodium transport. J. Clin. Invest. *52*, 2166–2174.

Sato, F., and Sato, K. (2000). cAMP-dependent Cl(-) channel protein (CFTR) and its mRNA are expressed in the secretory portion of human eccrine sweat gland. J. Histochem. Cytochem. *48*, 345–354.

Schön, M., Benwood, J., O'Connell-Willstaedt, T., and Rheinwald, J.G. (1999). Human sweat gland myoepithelial cells express a unique set of cytokeratins and reveal the potential for alternative epithelial and mesenchymal differentiation states in culture. J. Cell Sci. *112*, 1925–1936.

Shackleton, M., Vaillant, F., Simpson, K.J., Stingl, J., Smyth, G.K., Asselin-Labat, M.L., Wu, L., Lindeman, G.J., and Visvader, J.E. (2006). Generation of a functional mammary gland from a single stem cell. Nature *439*, 84–88.

Song, Y., Sonawane, N., and Verkman, A.S. (2002). Localization of aquaporin-5 in sweat glands and functional analysis using knockout mice. J. Physiol. *541*, 561–568.

Stingl, J., Eirew, P., Ricketson, I., Shackleton, M., Vaillant, F., Choi, D., Li, H.I., and Eaves, C.J. (2006). Purification and unique properties of mammary epithelial stem cells. Nature *439*, 993–997.

Tumbar, T., Guasch, G., Greco, V., Blanpain, C., Lowry, W.E., Rendl, M., and Fuchs, E. (2004). Defining the epithelial stem cell niche in skin. Science *303*, 359–363.

Van Keymeulen, A., Rocha, A.S., Ousset, M., Beck, B., Bouvencourt, G., Rock, J., Sharma, N., Dekoninck, S., and Blanpain, C. (2011). Distinct stem cells contribute to mammary gland development and maintenance. Nature *479*, 189–193.

Vasioukhin, V., Degenstein, L., Wise, B., and Fuchs, E. (1999). The magical touch: genome targeting in epidermal stem cells induced by tamoxifen application to mouse skin. Proc. Natl. Acad. Sci. USA *96*, 8551–8556.